Ukrainian Journal of Physical Optics
ISSUE 4
2026

STRUCTURAL, ELECTRONIC AND INFRARED PHOTOLUMINESCENCE PROPERTIES OF $Pb_{1-x}Eu_xTe$ THIN FILMS: EXPERIMENTAL AND FIRST-PRINCIPLES STUDY

M. A. MEHRABOVA [1,2], R. M. SADIGOV [1], Z. A. JAHANGIRLI [2,5], S. F. SAMADOV [2,3], A. S. ABIYEV [2,3,7], M. H. HASANOV [1], S. I. HASANOVA [8], S. G. ASADULLAYEVA [2,4,6]

[1] Azerbaijan Technical University, 25 Huseyn Javid Avenue, Baku, AZ1073, Azerbaijan
[2] Institute of Physics, Ministry of Science and Education, 131 Huseyn Javid Avenue, Baku, AZ1141, Azerbaijan
[3] Azerbaijan Architecture and Construction University, 5 Ayna Sultanova Street, Baku, AZ1073, Azerbaijan
[4] Azerbaijan State Oil and Industrial University, 41 Azadliq Avenue, Baku, AZ1010, Azerbaijan
[5] Baku State University, 33 Academician Zahid Khalilov Street, Baku, AZ1148, Baku, Azerbaijan
[6] Khazar University, 41 Mehseti St. Baku, AZ-1096, Azerbaijan
[7] Western Caspian University, 31 Istiglaliyyat Street, Baku 1001, Azerbaijan
[8] Azerbaijan University, 71 Jeyhun Hajibeyli Street, Baku AZ1007, Azerbaijan
*Corresponding author: saida.asadullayeva@asoiu.edu.az

Received: 06.08.2026

Abstract. $Pb_{1-x}Eu_xTe$ (x=0.1) thin films with a thickness of 1.5–2 μm were grown on glass and mica substrates by molecular beam condensation. X-ray diffraction revealed that the films crystallize mainly in the cubic PbTe phase with the $Fm\bar{3}$ space group, accompanied by a weak Eu-rich secondary phase with the $Pm\bar{3}$ space group. The substrate type strongly influenced the preferred orientation, with (200) texture observed on glass and (222) orientation on mica. Room-temperature photoluminescence measurements revealed pronounced infrared emission with three overlapping components centered at approximately 1779, 1811, and 1872 nm (0.697, 0.685, and 0.662 eV, respectively). The two higher-energy components are close to the ~0.70 eV band-gap value calculated for the $Pb_{0.875}Eu_{0.125}Te$ (x=0.125) model, whereas the lower-energy component extends into the sub-gap region. The observed emission is consistent with contributions from electronic states near the band edges and an additional lower-energy radiative channel, although room-temperature PL alone cannot unambiguously assign the individual emission mechanisms.

Keywords: PbEuTe thin films, photoluminescence, band structure, DFT, dielectric function
UDC: 535.373:539.23
DOI: 10.3116/16091833/Ukr.J.Phys.Opt.2026.04143

1. Introduction

Studying the optical and electronic properties of semiconducting materials is broadly significant in modern materials science and provides a fundamental basis for developing new functional materials [1–5]. In particular, narrow-bandgap semiconductors such as lead telluride (PbTe) attract attention due to their high thermoelectric efficiency, infrared light absorption capability, and tunable band structure [6–10]. $Pb_{1-x}Eu_xTe$ systems are of particular interest due to their modified electronic structure and infrared optical response associated with Eu incorporation [11–13]. Incorporating Eu into the PbTe matrix may introduce localized states and modify the electronic structure, thereby affecting the material's optical response. Previous studies have demonstrated that $Pb_{1-x}Eu_xTe$ systems exhibit composition-dependent electronic and optical characteristics, making them attractive for infrared optoelectronic applications [14–19]. Therefore, combined experimental and

theoretical investigations of their optical properties are essential for understanding their electronic behavior.

Photoluminescence (PL) spectroscopy provides valuable information about radiative recombination processes, defect-related states, and electronic transitions in semiconductor materials [19,20]. PL results can be correlated with theoretical calculations, particularly electronic band structures and optical functions from density functional theory (DFT), providing deeper insight into the material's fundamental properties [21,22]. Although $Pb_{1-x}Eu_xTe$ systems have been extensively studied, most previous reports have focused on epitaxial layers, quantum wells, or bulk crystals. Therefore, the influence of substrate type on the crystallographic texture and room-temperature infrared emission behavior of molecular-beam-condensed $Pb_{1-x}Eu_xTe$ thin films remains insufficiently explored. In this work, $Pb_{1-x}Eu_xTe$ (x = 0.1) thin films deposited on glass and mica substrates were investigated with particular emphasis on their room-temperature infrared photoluminescence. X-ray diffraction characterized the crystallographic structure and substrate-dependent texture, while first-principles calculations provided an electronic-structure framework for interpreting the observed PL emission. Particular attention was therefore given to the relationship between the measured infrared emission, the calculated electronic states, and the structural characteristics of the films.

Furthermore, we performed electronic structure calculations using the full-potential linearized augmented plane wave (FPLAPW) method within the density functional theory (DFT) framework, including the GGA+U approach and spin–orbit coupling (SOC), to clarify the electronic structure and the origin of the observed infrared emission. By combining experimental and theoretical approaches, this work provides insight into the relationship between substrate-dependent structural characteristics, Eu-related electronic states, and infrared emission behavior in $Pb_{1-x}Eu_xTe$ thin films.

2. Experimental and theoretical methods

In this work, thin films of $Pb_{1-x}Eu_xTe$ (x=0.1) with a thickness of 1.5–2 μm were grown on glass and mica substrates by the molecular beam condensation method in a vacuum of 10^{-4} Pa at a source temperature of T_{sour}=1000–1100 K and a substrate temperature of T_{sub}=580 K. Synthesized $Pb_{1-x}Eu_xTe$ (x=0.1) solid solutions were used as the evaporation source. We determined the film thickness (1.5–2 μm) using an MII-4 microinterferometer.

The crystal structure and phase composition of the $Pb_{1-x}Eu_xTe$ (x=0.1) solid solutions and thin films were investigated by X-ray diffraction (XRD) on a Bruker D2 Phaser (Germany) diffractometer using Cu Kα radiation, λ=1.54060 Å, selected by a curved graphite monochromator and a fixed divergence slit of 1/8°, in a Bragg–Brentano configuration.

Photoluminescence (PL) measurements were performed using a PL/PLE/Raman spectrometer (Tokyo Instruments, Inc.). We excited the samples with a 532 nm Nd:YAG laser. An MS3704i monochromator (SOL Instruments, Inc.) with a 100 grooves/mm diffraction grating dispersed the emitted radiation, which was detected using a DU491A-2.2 detector (Tokyo Instruments, Inc.). We considered the wavelength-dependent response of the detector–monochromator system during PL data analysis and corrected the measured spectra for instrumental response over the investigated infrared range (1650–2000 nm).

We calculated the electronic band structure, density of states, and dielectric functions using the full-potential linearized augmented plane wave (FPLAPW) method within density

functional theory (DFT), as implemented in the WIEN2k code. A detailed description of the calculation method is provided in [23,24].

3. Results and Discussion

3.1. Ab initio calculations

Fig. 1 shows the calculated band structure of PbTe using the GGA exchange-correlation potential [25]. We explicitly included SOC in the calculations because heavy Pb atoms make relativistic effects significant. In our calculations, the $Pb_{0.9}Eu_{0.1}Te$ structure was modeled using a 2×2×2 supercell (containing 64 atoms) of the primitive PbTe unit cell. This supercell consists of 28 Pb atoms, 32 Te atoms, and 4 Eu atoms substituting Pb sites, corresponding to a Eu concentration of x=0.125. This concentration is the closest achievable approximation to the experimental composition x=0.10 using integer atomic substitutions in the supercell approach. Given the proximity of the two compositions, the slightly higher Eu concentration in the model should produce a modest shift in the band gap, but it does not significantly affect the qualitative interpretation of the optical transitions.

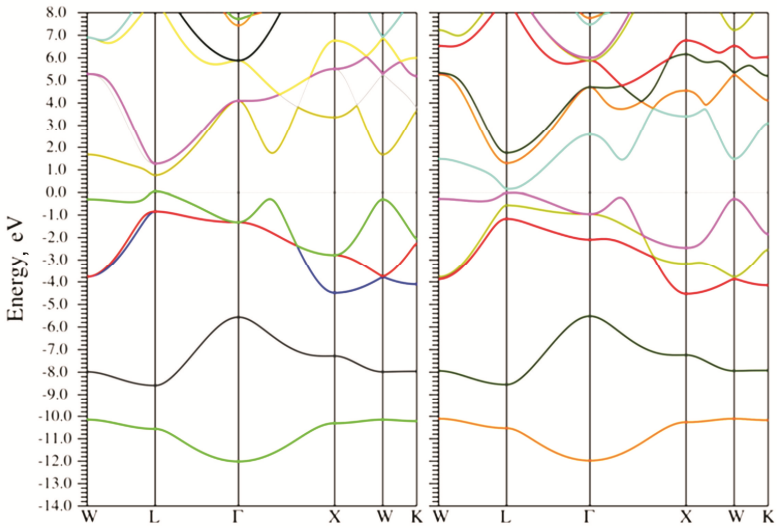

Fig. 1. Calculated electronic band structure of PbTe obtained within the GGA approximation: (left) without spin–orbit coupling (SOC) and (right) with SOC included. The Fermi level is set to the valence band maximum (VBM).

As shown in Fig. 1, PbTe exhibits a direct band gap located at the L high-symmetry point of the Brillouin zone. Without SOC (left panel), the valence and conduction bands show conventional dispersion with a relatively large band gap. However, when SOC is included (right panel), significant modifications in the band dispersion are observed, particularly near the valence band maximum and conduction band minimum. Including SOC produces pronounced splitting of both the valence and conduction bands, accompanied by a significant reduction in the band gap. These changes originate from strong relativistic effects associated with the heavy Pb atoms. In particular, SOC modifies the degeneracies of the electronic states and induces level repulsion between states of the same symmetry, shifting band energies and modifying the electronic band structure.

Consequently, the band dispersion and band-gap value change significantly. The band-gap-calculated SOC is 0.189 eV, which agrees well with the previously reported theoretical value of 0.22 eV [26] and the experimental band gap of 0.19 eV [27].

Fig. 2 presents the calculated electronic band structure of $Pb_{1-x}Eu_xTe$ (x=0.125) along the high-symmetry directions of the supercell Brillouin zone. The band structure calculated within the GGA+U approximation reveals significant modifications compared to pristine PbTe. For the GGA+U calculations, we applied a Coulomb parameter *U*=0.6 Ry for Eu. We adopted *U*=0.6 Ry for the Eu 4f states from previous GGA+U studies of Eu-containing chalcogenides and rare-earth compounds. This value reproduces the experimentally observed localization of Eu 4f states and yields a calculated band gap of ~0.70 eV. Including the on-site Coulomb interaction (*U*) for the localized Eu 4f states produces relatively flat bands in the valence and conduction regions, characteristic of strongly localized f-electron states.

The experimental crystal has a composition of x=0.10, while the computational model corresponds to x=0.125 (2×2×2 supercell). Despite this slight compositional difference (Δx=0.025), the calculated band gap of 0.70 eV is in excellent agreement with the experimental room-temperature PL emission peak range (0.685–0.696 eV), confirming that x=0.125 provides a reliable theoretical representation of the electronic structure and PL spectra near x=0.10.

Both the valence band maximum (VBM) and the absolute conduction band minimum (CBM) are located at the Γ-point. This indicates that $Pb_{1-x}Eu_xTe$ (x=0.125) is a direct-bandgap semiconductor with an approximate band gap of 0.7 eV. In pristine PbTe, the direct band gap is located at the L point of the primitive Brillouin zone, where both the VBM and CBM occur. For $Pb_{1-x}Eu_xTe$ (x=0.125), the electronic structure was calculated using a 2×2×2 supercell, resulting in a reduced Brillouin zone in which the L point of the primitive cell is folded onto the Γ point. Therefore, the appearance of both the VBM and CBM at Γ in the supercell representation is, in part, a consequence of Brillouin-zone folding and should not be interpreted as a literal displacement of the band extrema from L to Γ. The hybridization of localized Eu 4f and 5d orbitals with Pb p and Te p states modifies the band dispersion around Γ, establishing a true direct band gap of 0.7 eV for the alloyed composition.

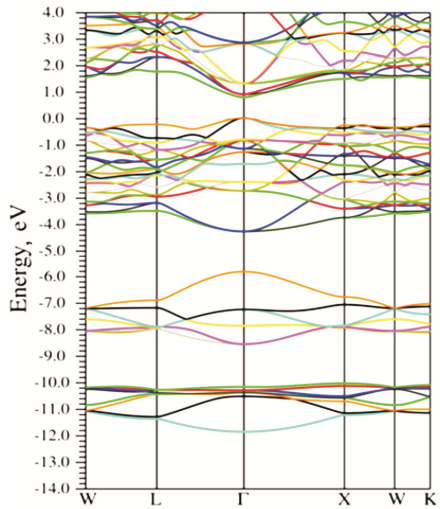

Fig. 2. Calculated electronic band structure of $Pb_{1-x}Eu_xTe$ (x=0.125, modeled using a 2×2×2 primitive supercell) obtained using the GGA+U approach. High-symmetry points refer to the supercell Brillouin zone, where the Γ-point corresponds to the folded L-point of pristine PbTe.

Fig. 3 presents the total density of states (DOS) and partial density of states (PDOS) for $Pb_{1-x}Eu_xTe$ (x=0.125). The PDOS analysis shows that the states near the valence band maximum are predominantly composed of Te p-states, with noticeable contributions from Pb s-states and localized Eu f-states. In contrast, the states near the conduction band minimum mainly originate from Pb p-states and Eu d-states, with a minor contribution from Te s-states. The presence of Eu introduces localized f-states into the electronic structure, which influence the band-edge characteristics while preserving the material's overall semiconducting behavior.

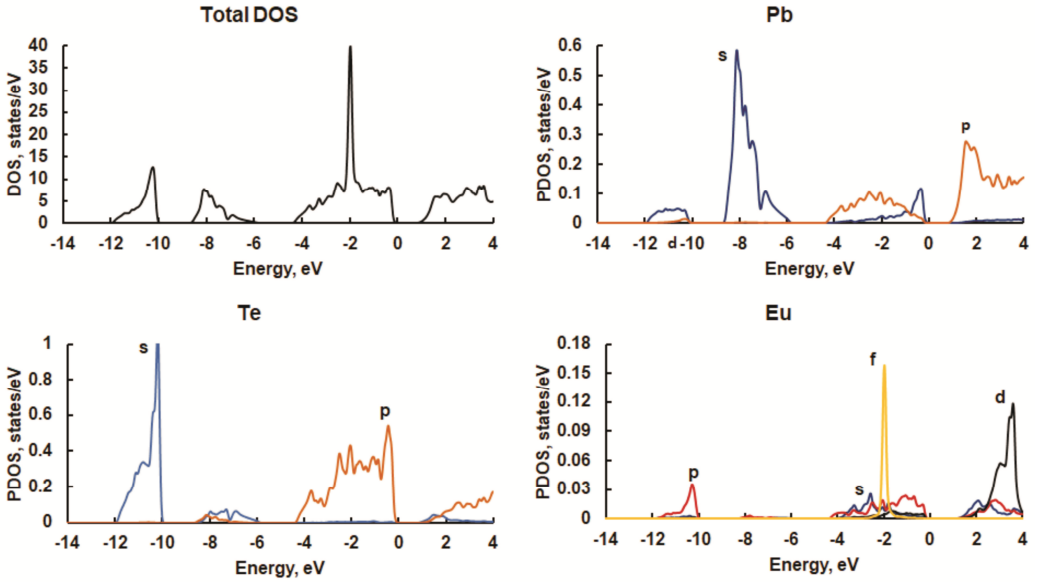

Fig. 3. Total and partial densities of states (DOS and PDOS) of Pb, Te, and Eu atoms in $Pb_{1-x}Eu_xTe$ (x=0.125). The Fermi level is set to the VBM.

The eigenvalues and eigenvectors obtained from the band structure calculations were used to compute the real and imaginary parts of the complex dielectric function (Fig. 4). The imaginary part of the dielectric function, Im ε(ω), exhibits a pronounced maximum at approximately 2.0 eV, which can be attributed to interband transitions from Pb s-, Te p-, and Eu f-states in the valence band to Pb p- and Eu d-states in the conduction band. The real part of the dielectric function, Re ε(ω), reaches its maximum at around 1.84 eV. The calculated static dielectric constant, Re ε(0), corresponding to the zero-frequency limit, is approximately 23. This relatively large value is consistent with the narrow band gap and strong interband transition effects characteristic of Pb-based chalcogenides.

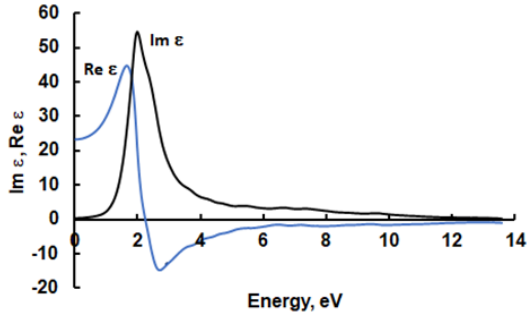

Fig. 4. Re ε and Im ε parts of the complex dielectric function of $Pb_{1-x}Eu_xTe$ (x=0.125) calculated within the GGA+U approach.

3.2. X-ray diffraction analysis

After deposition of the $Pb_{1-x}Eu_xTe$ (x=0.1) sample on different substrates, XRD analysis was performed. Previous studies at different concentrations have shown that the synthesis method, sample morphology, and dopant concentration strongly influence the formation of a single-phase material [28]. In particular, researchers have observed secondary-phase formation even at very low Eu concentrations. Compounds such as PbTe and EuTe normally crystallize in a cubic face-centered structure. In the present study, Eu^{2+} ions substitute Pb^{2+}

cations in the PbTe lattice. Several studies have reported that the ionic radius of Eu^{2+} is approximately 0.11 nm, while that of Pb^{2+} is about 0.12 nm. This indicates that Eu can be incorporated into the PbTe lattice [29–31].

These studies suggest that, although small changes in lattice parameters and structural distortions may occur after low-level substitution, the system can still remain single-phase. Wang et al. [32] reported that, under their sample preparation conditions, compositions with x≥0.03 exhibited XRD reflections from two cubic phases, $Pb_{1-x}Eu_xTe$ and $Eu_{1-x}Pb_xTe$, indicating the formation of an Eu-rich secondary phase. These findings suggest that an Eu-rich, EuTe-type secondary phase may also form in nominal $Pb_{0.9}Eu_{0.1}Te$. This interpretation is consistent with the XRD results obtained in the present study, since the investigated composition corresponds to x=0.1. Consequently, additional peaks associated with the secondary phase appear in the X-ray diffraction patterns of the sample.

The X-ray diffraction pattern of the $Pb_{1-x}Eu_xTe$ (x=0.1) sample deposited on glass is presented in Fig. 5. The diffraction pattern is dominated by the cubic PbTe phase with the $Fm\bar{3}$ space group (No. 225). According to the Rietveld refinement, the reflections corresponding to this phase account for approximately 98% of the total phase contribution. The fitting results indicate that enrichment of the system with Eu at x=0.1 promotes the formation of an additional intermetallic phase. The analysis shows that a small amount of a secondary PbEu phase, crystallized in the $Pm\bar{3}$ space group (No. 221), is present in the system.

As shown in Fig. 5, the PbTe phase deposited on the glass substrate exhibits a preferred orientation. Reflections corresponding to the (111), (200), (220), (311), (222), (400), (331), (420), (422), and (333) crystallographic planes are observed in the 2θ=10°–80° range. It is

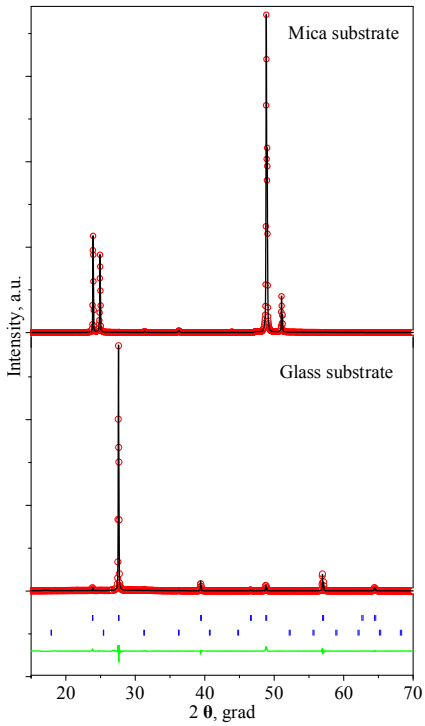

Fig. 5. X-ray diffraction spectra of $Pb_{1-x}Eu_xTe$ (x=0.1) thin films on different substrates: red corresponds to experimental results, black line to Rietveld refinement, green line to the calculated difference, and blue points to Bragg positions.

evident that the peak corresponding to the (200) plane exhibits an extremely high intensity. This feature indicates preferred orientation [33]. We quantitatively evaluated this preferred orientation using the exponential preferred-orientation correction implemented in FullProf during Rietveld refinement. Table 1 summarizes the quantitative results of the Rietveld refinement and preferred-orientation analysis. This phase is characterized by lattice parameters of a=6.462 Å and V=269.777 Å^3.

Fig. 6 shows the X-ray diffraction patterns of samples deposited on mica and glass substrates in the 2θ=20°–35° range, with peak intensities plotted on a $\log_{10}$ scale. The observed reflections indicate that the different substrates induce preferred orientations along different crystallographic directions.

Table 1. The quantitative results of the Rietveld refinement and preferred-orientation analysis.

Components	**Results**
Preferred orientation	[100], (200)
Profile Parameter, G_1	−16.64599 ± 0.67028
Profile Parameter, G_2	0.06755 ± 0.00135
Lattice parameter, a	6.4616 ± 0.0001 Å
Lattice volume, V	269.777 ± 0.003 Å^3
Profile R-factor, Rp	8.50%
Weighted profile R-factor, R_{wp}	13.9%
Expected R-factor, R_{exp}	4.65%
Goodness of fit, χ^2	8.92
Bragg R-factor, R_{Bragg}	3.29%

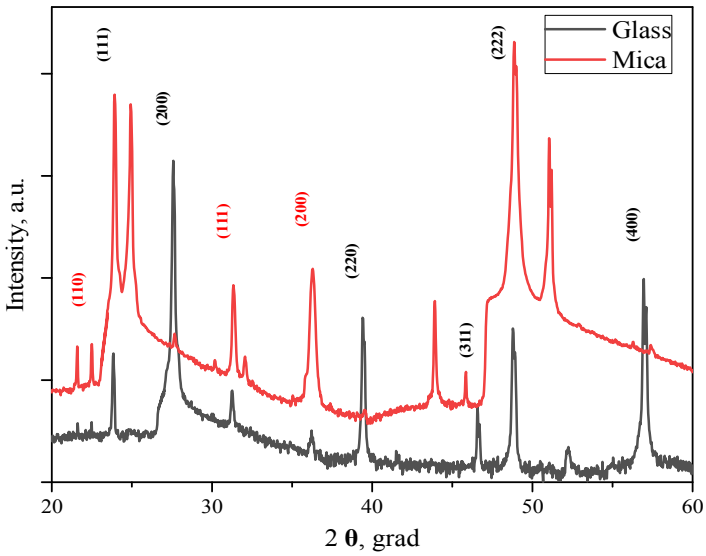

Fig. 6. X-ray diffraction patterns of $Pb_{1-x}Eu_xTe$ (x=0.1) samples deposited on different substrates, indexed with the corresponding Miller indices. The intensity scale is presented in $\log_{10}$ form. Red indices correspond to the Eu-rich secondary phase with the $Pm\bar{3}$ space group (No. 221), while black indices correspond to the PbTe phase with the space group (No. 225). In the sample deposited on the mica substrate, the PbTe phase with the $Fm\bar{3}$ space group exhibits long-range ordering with a preferred orientation along the (222) crystallographic direction [34]. In contrast, the intensity of the reflection corresponding to the (200) orientation remains significantly weaker than that of the former peak.

The substitution of Pb^{2+} by Eu^{2+} in the PbTe lattice is expected to preserve the cubic rock-salt PbTe-type structure because of the isovalent nature of the substitution. Although Eu^{2+} has an ionic radius comparable to that of Pb^{2+}, the lattice parameter of EuTe is larger than that of PbTe; therefore, the incorporation of Eu into the PbTe lattice may lead to a slight expansion of the cubic unit cell and a shift of the diffraction peaks toward lower 2θ values [35]. However, the results of the present study show that the lattice parameters do not change significantly and remain close in value. This indicates that only a limited amount of Eu is incorporated into the main PbTe phase. The Eu atoms that are not incorporated into the PbTe lattice may contribute to the formation of a secondary phase or local structural distortions [33].

3.3. Infrared photoluminescence

The room-temperature photoluminescence (PL) provides the main experimental evidence for the infrared optical response of the $Pb_{1-x}Eu_xTe$ (x = 0.1) thin films. As shown in Fig. 7, the films exhibit a pronounced infrared emission over the 1650–2000 nm spectral range under 532 nm excitation. The experimental spectrum can be described by three overlapping Gaussian emission components centered at 1778.9, 1810.7, and 1871.5 nm, corresponding to photon energies of approximately 0.697, 0.685, and 0.662 eV, respectively. We selected Gaussian functions because room-temperature emission in alloyed semiconductor thin films is dominated by inhomogeneous thermal and compositional broadening. Although weak modulation features are discernible on the flanks of the main bands (e.g., near 1720, 1760, 1820, 1860, and 1890 nm), adding sub-components to the room-temperature fit over-parameterizes the model due to thermal overlap (~25 meV). The fitted peak centers and widths with their respective standard uncertainties are: Component 1 at 1778.9±0.4 nm (FWHM=17.1±0.8 nm), Component 2 at 1810.7±0.6 nm (FWHM=29.0±1.2 nm), and Component 3 at 1871.5±1.1 nm (FWHM=45.7±2.3 nm). The relative integrated areas of the

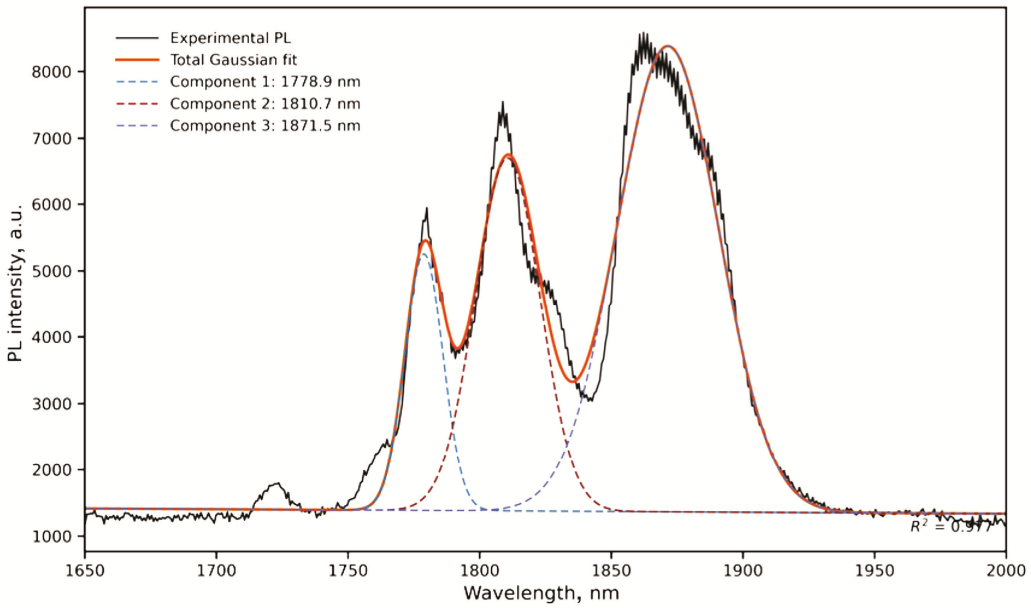

Fig. 7. Room-temperature infrared photoluminescence spectrum of $Pb_{1-x}Eu_xTe$ (x=0.1) thin films under 532 nm excitation. The experimental spectrum is shown together with the total three-component Gaussian fit and the individual fitted components. The fitted emission centers are 1778.9, 1810.7, and 1871.5 nm.

three components are approximately 12.2%, 28.5%, and 59.3%, respectively. The three-component fit well represents the measured spectrum (R^2=0.977).

A weak additional spectral feature is visible near 1725 nm on the high-energy side of the main emission. Because this feature is relatively weak and is not sufficiently resolved to justify an independent peak assignment, it is not included as a separate component in the present fitting analysis. We therefore treat it as a weak spectral contribution rather than as a distinct emission band. The most notable characteristic of the spectrum is the close energetic relationship between the higher-energy PL components and the electronic gap obtained from the first-principles calculations. The calculation was performed for $Pb_{0.875}Eu_{0.125}Te$ (x=0.125), whereas the experimental films have the composition $Pb_{0.9}Eu_{0.1}Te$ (x = 0.10). Thus, the calculated value of approximately 0.70 eV should be treated as a theoretical reference for comparison with the experimental PL rather than the exact calculated band gap for the investigated composition. Within this compositional difference, the fitted 1778.9 nm component (0.697 eV) is very close to the calculated band-gap value, while the 1810.7 nm component (0.685 eV) is also located in the same near-gap energy range. This energetic correspondence is consistent with a substantial contribution from electronic states near the band edges to the observed infrared emission. The agreement is particularly evident for the 1778.9 nm component, whose photon energy is close to the calculated ~0.70 eV gap. However, the energy agreement alone does not establish a unique microscopic recombination mechanism. Since the present measurements were performed only at room temperature, the observed bands cannot be unambiguously distinguished as direct band-to-band, excitonic, or shallow localized-state transitions. The two higher-energy components are therefore more appropriately described as emission contributions associated with the near-band-edge energy region.

The third fitted component is broader and shifted to lower energy, centered at 1871.5 nm (0.662 eV) with an FWHM of 45.7 nm. Its lower photon energy relative to the calculated ~0.70 eV gap is consistent with an additional sub-gap radiative contribution. Such emission may be associated with localized electronic states within the gap or with local electronic environments arising from compositional and structural disorder. Eu-related electronic states, intrinsic defects, and other local structural variations are possible contributors, but the present PL data do not allow these possibilities to be distinguished reliably. For this reason, we do not assign the 1871.5 nm component to a specific defect or Eu-related transition.

The relative integrated intensities provide additional information about the PL response. The broad lower-energy component accounts for the largest fraction of the fitted emission area, approximately 59%, while the 1810.7 nm and 1778.9 nm components contribute approximately 29% and 12%, respectively. This result shows that the fitted emission area is dominated by the lower-energy component. Nevertheless, the relative intensity of a PL component cannot, by itself, be taken as direct evidence for a particular microscopic state, because measured intensity can be influenced by the population and recombination probability of the corresponding states, as well as by spectral broadening and experimental response. The structural characteristics of the films provide a possible context for the coexistence of these emission contributions. XRD indicates substrate-dependent crystallographic texture and a weak secondary phase, while electronic-structure calculations show that Eu incorporation modifies states near the band edges. These

factors may alter the local electronic environment and consequently the available radiative recombination pathways. However, the present data do not establish a direct correspondence between a particular structural feature and an individual PL component.

Taken together, the PL measurements demonstrate pronounced room-temperature infrared emission from $Pb_{1-x}Eu_xTe$ thin films and reveal at least three overlapping radiative contributions. The two higher-energy components occur close to the calculated band-gap reference for the x = 0.125 model, whereas the broad lower-energy component extends into the sub-gap region. The results therefore support a significant contribution from electronic states near the band edges together with an additional lower-energy radiative channel. Definitively identifying the microscopic origin of the individual emission components will require complementary measurements, particularly temperature-dependent, excitation-power-dependent, and time-resolved PL spectroscopy.

4. Conclusion

This study shows that $Pb_{1-x}Eu_xTe$ (x=0.1) thin films retain the dominant cubic PbTe-type structure with the $Fm\bar{3}$ space group after deposition. XRD confirms that Eu incorporation does not cause a complete structural transformation of the PbTe matrix; however, the appearance of a weak secondary PbEu phase indicates limited Eu solubility in the main lattice. The substrate type was found to play an important role in the crystallographic orientation of the films, producing a strong (200) preferred orientation on glass and a dominant (222) orientation on mica. The combined structural, photoluminescence, and theoretical results show that Eu incorporation modifies the electronic structure of the PbTe matrix and is accompanied by pronounced room-temperature infrared emission. The PL spectrum consists of three overlapping emission components, with the two higher-energy components lying close to the calculated band-gap reference for the x=0.125 model, while the broader lower-energy component extends into the sub-gap region. These results support a contribution from electronic states near the band edges together with an additional lower-energy radiative channel. However, room-temperature PL alone cannot unambiguously assign the individual emission mechanisms. Further temperature-dependent, excitation-power-dependent, and time-resolved PL measurements would help clarify the microscopic origin of the observed emission features.

Disclosures. The authors declare no conflicts of interest.

Funding. This research received no specific grant from any funding agency in the public, commercial, or not-for-profit sectors.

Authors' contributions. M.A. Mehrabova: conceptualization, supervision. R.M. Sadigov: sample growth, XRD measurements. Z.A. Jahangirli: DFT calculations, band structure analysis, formal analysis. S.F. Samadov: writing – original draft, XRD analysis. A.S. Abiyev: XRD analysis. M.H. Hasanov: PL analysis. S.I. Hasanova: literature review. S.G. Asadullayeva: photoluminescence measurements, writing – review editing, correspondence.

References

1. Nuriyev, I. R., Mehrabova, M. A., Nazarov, A. M., & Sadigov, R. M. (2016). Growth of epitaxial $Cd_{1-x}Mn_xTe$ films. *Inorganic Materials*, *52*, 886–889.
2. Mekhrabov, A. O., & Mehrabova, M. A. (2024). Effect of gamma irradiation on structural and optical properties of CdMnTe epitaxial thin films. *Materials Science Forum*, *1119*, 3–12.

3. Nuriyev, I. R., Mehrabova, M. A., & Hasanov, N. H. (2018). Structure and surface morphology of $Cd_{1-x}Mn_xTe$ epitaxial films. *Journal of Surface Investigation*, *12*, 504–506.
4. Nuriyev, I. R., Mehrabova, M. A., Nazarov, A. M., Sadigov, R. M., & Hasanov, N. H. (2017). On the growth, structure, and surface morphology of epitaxial CdTe films. Semiconductors, *51*, 34–37.
5. Mehrabova, M. A., & Madatov, R. S. (2011). Calculation of the electron structure of vacancies and their compensated states in III–VI semiconductors. *Semiconductors*, *45*, 998–1005.
6. Suzuki, N., & Adachi, S. (1994). Optical properties of PbTe. *Japanese Journal of Applied Physics*, *33*, 193–198.
7. Ekuma, C. E., Singh, D. J., Moreno, J., & Jarrell, M. (2012). Optical properties of PbTe and PbSe. *Physical Review B*, *85*, 085205.
8. Kungumadevi, L., & Sathyamoorthy, R. (2012). Structural, electrical, and optical properties of PbTe thin films prepared by simple flash evaporation method. *Advances in Condensed Matter Physics*, *2012*, 763209.
9. Zhong, Y., Tang, J., Liu, H., Chen, Z., Lin, L., Ren, D., Liu, B., & Ang, R. (2020). Optimized strategies for advancing n-type PbTe thermoelectrics: A review. *ACS Applied Materials & Interfaces*, *12*, 49323–49334.
10. Rogacheva, E. I., Nashchekina, O. N., & Menshikova, S. I. (2017). Size effects in transport properties of PbSe thin films. *Journal of Electronic Materials*, *46*, 3842–3850.
11. Trajic, J., Romcevic, M., Romcevic, N., Nikolic, S., Golubovic, A., Duric, S., & Nikiforov, V. N. (2004). Optical properties of PbTe:Mn. *Journal of Alloys and Compounds*, *365*, 89–93.
12. Ismayilova, N. A., & Abiyev, A. S. (2026). Comprehensive first-principles engineering of TM-doped InP nanosheets for multifunctional device platforms: Spintronics and optoelectronics International. *Journal of Modern Physics B*, *40*, 2650164.
13. Hu, Z.-K., & Chen, S.-W. (2022). Interfacial reactions in Cu/PbTe and Cu/PbSe couples. *Journal of Alloys and Compounds*, *899*, 163299.
14. Tian, Z., Garg, J., Esfarjani, K., Shiga, T., Shiomi, J., & Chen, G. (2012). Phonon conduction in PbSe, PbTe, and $PbTe_{1-x}Se_x$ from first-principles calculations. *Physical Review B*, *85*, 184303.
15. Jia, B. H., Jiang, B. B., & He, J. Q. (2019). Recent advances of n-type low-cost PbSe-based thermoelectric materials. *Materials Today Advances*, *4*, 100029.
16. Abramof, E., Rappl, P. H. O., Ueta, A. Y., Motisuke, P.& Ferreira, S. O. (1999). PbEuTe/PbTe multi-quantum wells: Structural and optical properties. *MRS Online Proceedings Library*, *607*, 339.
17. Yuan, S., Krenn, H., Springholz, G., Ueta, Y., Bauer, G., & McCann, P. J. (1997). Magnetoreflectivity of $Pb_{1-x}Eu_xTe$ epilayers and $PbTe/Pb_{1-x}Eu_xTe$ multiple quantum wells. *Physical Review B*, *55*, 4607–4619.
18. Gibbs, Z. M., Kim, H., Wang, H., White, R. L., Drymiotis, F., Kaviany, M., & Snyder, G. J. (2013). Temperature dependent band gap in PbX (X = S, Se, Te). *Applied Physics Letters*, *103*, 262109.
19. Braunstein, G., Dresselhaus, G., Heremans, J., & Partin, D. (1987). Magnetic properties of $Pb_{1-x}Eu_xTe$ grown by molecular-beam epitaxy. *Physical Review B*, *35*, 1969–1972.
20. Pashkeev, D. A., Selivanov, Yu. G., Felder, F., & Zasavitskii, I. I. (2010). Dependence of photoluminescence spectra of epitaxial $Pb_{1-x}Eu_xTe$ ($0 \le x \le 0.1$) alloy layers on conditions of growth. *Semiconductors*, *44*, 861–866.
21. Jahangirli, Z. A., Asadullayeva, S. G., Amiraslanov, I. R., Eyyubov, Q. Y., Rahimli, A. B., & Abiyev, A. S. (2025). Ab initio and experimental investigations of the electronic and optical properties of pure and p-aminopyridine-intercalated $In_{1.2}Ga_{0.8}S_3$. *Indian Journal of Physics*, *99*, 2087–2092.
22. Asadullayeva, S. G., Jahangirli, Z. A., Naghiyev, T. G., & Abiyev, A. S. (2025). Systematic analysis of the optical properties of $ZnGa_2Se_4$ single crystal. *Current Applied Physics*, *76*, 39–44.
23. Asadullayeva, S. G., & Jahangirli, Z. A. (2025). Photoluminescence and magnetic properties of Nd-doped ZnGa2Se4. *European Physical Journal B*, *98*, 142.
24. Blaha, P., Schwarz, K., Madsen, G. K. H., Kvasnicka, D., & Luitz, J. (2001). *WIEN2k: An augmented plane wave plus local orbitals program for calculating crystal properties*. Technische Universität Wien.
25. Perdew, J. P., Burke, K., & Ernzerhof, M. (1996). Generalized gradient approximation made simple. *Physical Review Letters*, *77*, 3865–3868.
26. Xu, L., Zheng, Y., & Zheng, J.-C. (2010). Thermoelectric transport properties of PbTe under pressure. *Physical Review B*, *82*, 195102.
27. Zhang, Y., Ke, X., Chen, C., Yang, J., & Kent, P. R. C. (2009). Thermodynamic properties of PbTe, PbSe, and PbS. *Physical Review B*, *80*, 024304.
28. Chen, Z., Jian, Z., Li, W., Chang, Y., Ge, B., Hanus, R., Yang, J., Chen, Y., Huang, M., Snyder, G. J., & Pei, Y. (2017). Lattice dislocations enhancing thermoelectric PbTe in addition to band convergence. *Advanced Materials*, *29*, 1606768.
29. Gromovoj, Yu. S., Plyatsko, S. V., & Kostyunin, G. E. (1992). The superhyperfine structure in the EPR spectra of Eu^{2+} ions in PbTe films. *Materials Letters*, *13*, 18–20.

30. Górska, M., Anderson, J. R., Peng, J. L., Oka, Y., Jen, J. Y., Mogi, I., Ravot, D., & Gołacki, Z. (1997). Concentration dependence of the exchange interaction in $Pb_{1-x}Eu_xTe$. *Physical Review B*, *55*, 4400–4404.
31. Pirralho, M. J. P., Peres, M. L., Soares, D. A. W., Braga, P. C. O., Pena, F. S., Fornari, C. I., Rappl, P. H. O., & Abramof, E. (2017). Transition from negative to positive photoconductivity in p-type $Pb_{1-x}Eu_xTe$ films. *Physical Review B*, *95*, 075202.
32. Wang, X., Veremchuk, I., Bobnar, M., Zhao, J., & Grin, Y. (2016). Solid solution $Pb_{1-x}Eu_xTe$: Constitution and thermoelectric behavior. *Inorganic Chemistry Frontiers*, *3*, 1152–1159.
33. Krataitong, C., Srichai, K., & Tubtimtae, A. (2021). Structural and optical properties of undoped and antimony-doped lead telluride thin films. *Materials Letters*, *285*, 129085.
34. Miracle, J., Nichols, A., Cantrell, S., Myers, T., & Theodoropoulou, N. (2026). Epitaxial growth and structural characterization of PbTe thin films on CdTe(211)B: Evidence of a 180° twisted interface. *Crystal Growth & Design*, *26*, 3267–3275.
35. Smajek, E., Szot, M., Kowalczyk, L., Domukhovski, V., Taliashvili, B., Dziawa, P., Knoff, W., Łusakowska, E., Reszka, A., Kowalski, B., Wiater, M., Wojtowicz, T., & Story, T. (2011). Optical and structural properties of $Pb_{1-x}Eu_xTe$/CdTe//GaAs (001) heterostructures grown by MBE. *Journal of Crystal Growth*, *323*, 140–143.
36. Goltsos, W., Nakahara, J., Nurmikko, A. V., & Partin, D. L. (1985). Photoluminescence in PbTe–PbEuTeSe multiquantum wells. *Applied Physics Letters*, *46*, 1173–1175.
37. Springholz, G., Kriechbaum, M., Hofmann, W., Geist, F., Pascher, H., Yuan, S., Krenn, H., & Bauer, G. (1993). Photoluminescence of semimagnetic PbEuTe/PbTe quantum wells in magnetic fields. *Superlattices and Microstructures*, *13*, 25–28.
38. Samadov, S. F., Ismayilova, N., Popov, E., Tuyen, L. A., Trung, N. V. M., Samedov, O. A., Sidorin, A. A., Orlov, O. S., Jabarov, S., Hue, P. T., Hue, N. T. N., Tiep, N. V., Hung, N. Q., & Mirzayev, M. N. (2026). Gamma-irradiation-induced defects and thermally driven recovery in ZrB_2. *Materials Chemistry and Physics*, *353*, 132107.

Mehrabova, M. A., Sadigov, R. M., Jahangirli, Z. A., Samadov, S. F., Abiyev, A. S., Hasanov, M. H., Hasanova, S. I., Asadullayeva, S. G. (2026). Structural, Electronic and Infrared Photoluminescence Properties of $Pb_{1-x}Eu_xTe$ Thin Films: Experimental and First-Principles Study. *Ukrainian Journal of Physical Optics*, *27*(4), 04143 – 04154.
doi: 0.3116/16091833/Ukr.J.Phys.Opt.2026.04143

Анотація. *В роботі були отримані тонкі плівки $Pb_{1-x}Eu_xTe$ (x=0,1) товщиною 1,5–2 мкм методом конденсації молекулярних пучків на підкладках зі скла та слюди. Методом рентгенівської дифракції було встановлено, що плівки кристалізуються переважно в кубічній фазі PbTe із просторовою групою $Fm\bar{3}$. Також виявлено слабку вторинну фазу, збагачену європієм, із просторовою групою $Pm\bar{3}$. Тип підкладки суттєво впливав на переважну орієнтацію: на склі спостерігалася орієнтація (200), а на слюді — (222). При вимірюванні фотолюмінесценції за кімнатної температури було виявлено виражене інфрачервоне випромінювання, що складається з трьох компонент із максимумами приблизно при 1779, 1811 та 1872 нм (відповідно 0,697; 0,685 та 0,662 еВ), які перекриваються. Дві високоенергетичні компоненти близькі до значення ширини забороненої зони (~0,70 еВ), розрахованої для моделі $Pb_{0,875}Eu_{0,125}Te$ (x=0,125), тоді як низькоенергетична компонента проявляється в області енергій, менших за ширину забороненої зони. Спостережуване випромінювання узгоджується з внеском електронних станів поблизу країв зон та додатковим низькоенергетичним каналом випромінювальної рекомбінації. Однак самі лише дані фотолюмінесценції за кімнатної температури не дозволяють однозначно ідентифікувати окремі механізми випромінювання.*

Ключові слова: *тонкі плівки PbEuTe, фотолюмінесценція, зонна структура, DFT, діелектрична функція*